Diagnosis of Ocean Near-Surface Horizontal Momentum Balance from pre-SWOT altimetric data, drifter trajectories, and wind reanalysis

Margot Demol[1], Aurélien L. Ponte[1], Pierre Garreau[1], Jean-François Piollé[1], Clément Ubelmann[2], Nicolas Rascle [1]

[1]Ifremer, LOPS, Plouzané, France
[2]Datlas, Grenoble, France

Key Points:

- Horizontal ocean surface momentum reconstruction from colocated drifters and along-track altimetric data gives closure of up to 80%.
- Ageostrophic dynamics account for about one third of the global balanced momentum variance.
- Errors preventing closure are mainly resolution mismatch errors, followed by colocation and instrumental errors.

Corresponding author: Margot Demol, margot.demol@ifremer.fr

Abstract

Along-track and gridded altimetric observations of sea level are colocated and combined with data from drifter observations and wind reanalysis to reconstruct global instantaneous near-surface horizontal momentum balance. This reconstruction includes not only geostrophic terms, but also Lagrangian accelerative terms and turbulent stress terms. The methodology developed quantifies the degree of closure, distinguishes balanced signals from errors, and estimates dynamical compensation between pairs of terms. Overall, the residual variance of the momentum balance is about 20% of the sum of individual terms variance. We carry out a detailed exploration of the misclosure, which is dominated by unbalanced signals in drifter observations (resolution mismatch accounts for 41% of the total error), followed by instrumental and spatial colocation errors. Although geostrophy is the leading order equilibrium, ageostrophic contributions associated with non-linear balanced motions, internal tides and near-inertial waves account for one third of the global balanced signal variance. Momentum balance reconstructions and the methodology developed here for that purpose hold promise for validating SWOT sea level observations, for quantifying our ability to estimate the ocean circulation from these observations, and for improving our understanding of ocean near-surface dynamics.

Plain Language Summary

Estimates of the ocean surface circulation are routinely gleaned from sea level measurements, based on the assumption of a balance between the Coriolis force felt by any moving object (including water parcels) traveling at the surface of Earth and the force induced by spatial variations in sea level. Due to its unprecedented resolution, sea level observations from the new satellite-based Surface Water Ocean Topography (SWOT) survey led by NASA and CNES will contain substantial signatures from high-frequency or shorter-scale motions, where the equilibrium between these two forces is disrupted. These disruptions hinder our ability to make accurate predictions of ocean surface currents from sea level measurements. Other sources of observation are required to reconstruct the ocean surface dynamics more completely. In this paper, we supplement pre-SWOT altimetric data with surface drifter trajectory data and a wind reanalysis product to diagnose the ocean surface dynamical equilibrium beyond geostrophy. Our approach indicates that one third of the global dynamical balance is due to forces that are ignored in the two-force geostrophic balance. We quantify different sources of error that prevent perfect dynamical closure. Our approach will help take full advantage of SWOT sea level measurements.

1 Introduction

Near-surface ocean variability plays a pivotal role in regulating air-sea interactions and ocean circulation, which in turn redistribute heat and all ocean-suspended materials. A comprehensive study of this variability is therefore essential for understanding and forecasting the evolution of the ocean on climatic scales (Ferrari, 2011; Cronin et al., 2019; Elipot & Wenegrat, 2021). The physical and geochemical environment (e.g. nutrient availability) is subject to significant control by near-surface dynamics, which in turn exert a strong influence on the development of marine life, and ultimately affect human activities (Taylor & Ferrari, 2011; Lévy et al., 2018). More thorough knowledge and more precise modeling of surface ocean dynamics can facilitate more accurate operational estimations of the ocean surface circulation with numerous potential applications including rescue strategies, oil spill containment, forecasting of plastic drift, and enhanced environmental management (Röhrs et al., 2023).

The dynamics of the near-surface ocean is complex, resulting from a combination of a large range of interacting processes characterized by different temporal and spatial scales. These processes include mesoscale eddies with O(100 km) horizontal scales, submesoscale motions with O(10 km) horizontal scales, internal tides and Lagrangian waves (100 km-1 km), and quasi three-dimensional turbulence scales (1-10 m). At small Rossby numbers i.e. large spatial scales and slow motions, near-surface dynamics reduce to the so-called geostrophic balance between the pressure gradient force and the Coriolis force. Under this regime, sea level observations provide access to ocean surface currents. However, for a more accurate reconstruction, the vertical redistribution of momentum induced by surface winds can be taken into account using Ekman models, for instance (Ekman and Vagn Walfrid (1905)). In addition, high-frequency and shorter-scale wave-like motions, such as internal tides and wind-driven near-inertial waves, do not obey geostrophic balance and require the integration of accelerative and/or advective effects (Yu et al., 2021).

In recent decades, advancements in observational capabilities have enhanced our understanding of the various processes that contribute to near-surface ocean dynamics. Up to the 1980s, efforts to reconstruct near-surface ocean dynamics relied on local in situ measurements (e.g. moorings or oceanographic cruises). These efforts yielded results that were in good agreement with a Lagrangian-geostrophic-Ekman balance (Davis et al., 1981; Johnson & Luther, 1994). The addition of satellite-based Global Positioning System (GPS) for tracking drifting devices in the 1970s and the advent of altimetric satellite missions in the late 1980s paved the way for investigations of near-surface dynamical balances at the global scale. Later, in the 2000s, reconstructions of Ekman-geostrophic momentum balance from these improved observations of sea level, gravity, drifter velocities, and surface winds allowed to assess these observations and to estimate the first global mean dynamic topography (MDT), defined as the contribution to spatial sea level fluctuations that is in balance with the mean surface circulation (Niiler et al., 2003; Rio & Hernandez, 2004).

Over the past decade, advancements in altimetric satellite accuracy have enabled the resolution of features with spatial scales of approximately 65 km in along-track observations (Dufau et al., 2016; Stammer & Cazenave, 2017). Furthermore, the precision and resolution of drifter tracking have also improved, resulting in the production of an hourly low-noise global dataset of surface currents (Elipot et al., 2016). These improved observations have led to refined MDT products (Maximenko et al., 2009; Rio et al., 2011; Mulet et al., 2021). The recently launched altimetric satellite-based Surface Water and Ocean Topography (SWOT) survey is now providing observations of sea level with unprecedented resolution (estimated 2 km) and coverage owing to its wide-swath capability.

These successive enhancements in observation capabilities can capture motions that require going beyond geostrophy. Laying the groundwork for SWOT data, this study aims to diagnose global ocean surface dynamics by reconstructing instantaneous horizontal momentum conservation (i.e estimating and combining the different terms), from along-track altimetry and colocated drifter and wind observations, thereby capturing high-frequency and submesoscale contributions. The novelty of this work lies in the use of a set of colocated observations rather than geographically gridded products. We compare the use of along-track and gridded altimetry. We set out to answer the three following questions:

1. What is the capacity of pre-SWOT observations to close the upper ocean horizontal momentum budget ?
2. How do all dynamical terms quantitatively and geographically contribute to the closure of near-surface ocean dynamics?
3. What are the sources of misclosure in momentum conservation?

The article is organized as follows. Section 2 presents the data and statistical methods employed to reconstruct and diagnose surface momentum balance from observations. Section 3.1 presents the global diagnosis of closure and dynamical contributions. Sources of misclosure are investigated in Section 3.2. Geographical modulations of these results are the subject of Section 3.3.

2 Materials and methods

2.1 Materials

Surface momentum conservation was reconstructed over the 2010-2020 period based on a combination of surface drifter trajectories, altimetric observations and surface wind stress reanalysis. The hourly dataset from the Global Drifter Program (GDP) (Elipot et al., 2016) provides observations of surface currents and acceleration. GDP drifters are tracked using two different positioning systems (i.e. GPS and Argos), which differ in their accuracy. GDP drifter displacements are assumed representative of water motion at 15 m depth when drifters still possess their drogues. However, a drifter always loses its drogue after some time, then becoming more influenced by wind drift (Poulain et al., 2009). Sensitivity analyses presented in Appendix A motivate the following choices: 1/ only drogued drifter data are considered; 2/ a 2.5 cpd low-pass filter is applied to drifter data to minimize contamination of acceleration estimates by positional noise; 3/ GPS and Argos drifters are both considered, because the 2.5 cpd low-pass filter effectively mitigates the greater noise level in the Argos tracking data.

Altimetric data comprises along-track L3 data where we consider sea level anomalies (SLA), MDT (see Stammer and Cazenave (2017) for proper definitions), and barotropic and internal tide corrections for Jason-2, Jason-3, Cryosat-2, Sentinel-3A, and Sentinel-3B satellite tracks. Along-track SLA effectively resolve processes with wavelengths down to $\sim$65 km in mid-latitudes areas, but have limited spatial coverage inherent to along-track observations (Dufau et al., 2016). We also consider AVISO-gridded SLA which are provided daily at a 1/25° resolution around the globe. The AVISO SLA are estimated with optimal interpolation using L3 along-track observations from all altimetric missions available. Its mean effective spatial resolution is lower than that of along-track observations, resolving scales of $\sim$200 km at mid-latitudes (Ballarotta et al., 2019).

The ERA* dataset contains hourly and 1/25° wind stress data (Trindade et al., 2020). This dataset is a data assimilation reanalysis product corrected with geolocated scatterometers, and presumably takes into account processes that were absent or misrepresented in the original model (e.g. strong current effects, wind effects associated with mesoscales, coastal effects, and large-scale circulation effects) (Portabella et al., 2021).

2.2 Building a colocated dataset

This study is based on colocations between different observations (Figure 1). AVISO and ERA* are gridded products; both allow interpolation and therefore do not constitute constraints. In contrast, along-track altimetry and drifter trajectory observations are spatially and temporally sparser. Matchup points where both are available were therefore identified with prescribed temporal and spatial mismatch tolerances denoted as ΔT and ΔX, respectively, for what we call drifter-matchup and altimeter-matchup points.

Given the hourly resolution of drifter data, a temporal mismatch ΔT of 30 min was selected. This temporal mismatch is small compared with the characteristic time scales of the geophysical signals of interest, namely inertial or tidal periods. Therefore, this mismatch does not yield substantial temporal colocation errors (Figure S1 in Supporting Information). A spatial mismatch tolerance of 25 km was chosen. It represents a trade-off between the number of available colocations and thus the resulting statistical reliability and accumulation of colocation errors with spatial mismatch (see Section 3.2.1). With this spatial mismatch of 25 km, the statistical errors on the momentum residual mean square were less than 50% of its value in 86% of the ocean 5°-geographical bins (Figure S2 in Supporting Information).

The total number of colocations for these given tolerances is about 239,000.

2.3 Reconstructing horizontal along-track momentum conservation

We then used this colocation dataset to reconstruct the horizontal surface momentum conservation equation in the altimeter along-track direction (x-axis):

$$\underbrace{\overbrace{d_t u \qquad -fv}^{\substack{\text{Lagrangian and Coriolis}\\ \text{accelerations}}}}_{\text{GDP drifters}} + \underbrace{\overbrace{g\partial_x \eta}^{\substack{\text{Pressure}\\ \text{gradient term}}}}_{\substack{\text{Along-track}\\ \text{+ AVISO altimetry}}} - \underbrace{\overbrace{\frac{1}{\rho_0}\partial_z \tau_x}^{\substack{\text{Wind term}\\ \text{Vertical stress divergence}}}}_{\text{ERA*}} = \overbrace{\epsilon}^{\text{Residual}} , \qquad (1)$$

where d_t is the material time derivative, f the Coriolis frequency, u and v the along-track and cross-track velocities, respectively, g gravity, η introduced as the Dynamic Sea Level (DSL), ρ_0 the seawater density (considered constant), and τ_x the along-track turbulent stress. The residual ϵ is composed of several different possible errors, such as missing physics or estimation process errors, which will be examined in Section 3.2.

The surface momentum conservation (1) includes terms involved in the geostrophic balance, namely Coriolis acceleration and the pressure gradient term, but also two ageostrophic terms, namely Lagrangian acceleration and vertical turbulent stress divergence. Note that Eulerian advective terms are accounted for in the Lagrangian acceleration. The quantification of the contributions of these two ageostrophic terms is one of our main focus here.

For each colocation, all terms on the left-hand side of (1) are estimated from observations as follows:

1. GDP-filtered velocities are rotated in the along-track/cross-track directions and provide estimates of the Coriolis acceleration ($-fv$) and Lagrangian acceleration ($d_t u$) via centered time differentiation.
2. The pressure gradient term can be estimated in three ways, giving three different reconstructions that we compare:
   (a) along-track reconstruction: the pressure gradient term is estimated from along-track altimetry at the altimeter-matchup point;
   (b) altimeter-matchup AVISO reconstruction: the pressure gradient term is estimated from AVISO altimetry interpolated at the altimeter-matchup point, i.e. with the same spatial mismatch as along-track altimetry;
   (c) drifter-matchup AVISO reconstruction: the pressure gradient term is estimated from AVISO altimetry, but interpolated at the drifter-matchup point, thus with no spatial mismatch.

   In all cases, DSL η was estimated from the sum of SLA and MDT. Along-track reconstruction DSL values account for ocean tides and internal tide signals, because we added the related corrections back in. We were not able to do so for AVISO reconstructions, because these corrections are not available in the product. DSL was then differentiated to provide an estimate of the pressure gradient term ($g\partial_x\eta$). The AVISO DSL spatial gradient in the along-track direction was linearly interpolated at the drifter-matchup or altimeter-matchup position and time.
3. ERA* wind stress was spatially and temporally linearly interpolated at the drifter-matchup point. This surface wind stress was then extrapolated into vertical stress

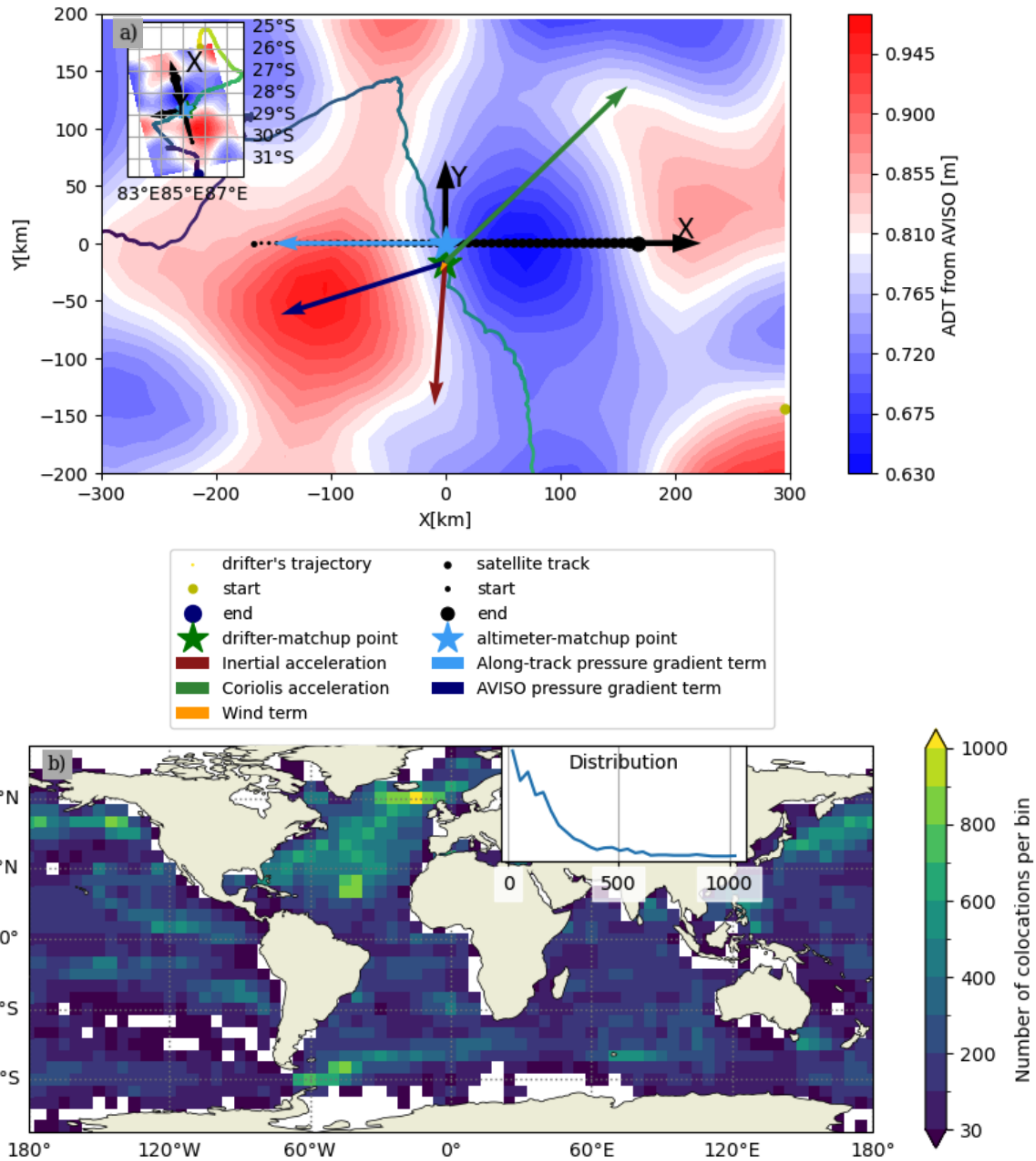

Figure 1. a) Example of a colocation: a drifter trajectory crossing a nadir satellite track in the local coordinates and in the longitude-latitude coordinates (inset). The different terms of the momentum equation (arrows) are estimated either at the drifter-matchup point or at the altimeter-matchup point (stars), which are separated by a ΔX spatial mismatch of 17 km and a ΔT temporal mismatch of 20 min for the represented colocation. The drifter trajectory is represented for 2 months centered around the matchup date. The nadir satellite track is also represented with measurement points on either side of the altimeter-matchup point, measurements being separated by approximately 7 km. The local coordinate system is defined with the along-track x-axis and the cross-track y-axis (black arrows). AVISO absolute dynamic topography (i.e. the sum of MDT and SLA) is interpolated over a 400 km long x 200 km wide x-y oriented box with a spatial resolution of 5 km and used here as a background. Note that, in contrast to the other terms, only the along-track pressure gradient component can be computed and represented here. b) Geographical distribution of colocations in 5°-geographical bins. The inset shows the distribution of the number of colocations per bin.

divergence at 15 m using the Rio et al. (2014) empirical Ekman model with their global 15-m parameters β_{ek} and θ_{ek} (0.25 $m^2.s.kg^{-1}$ and $\pm 48.18°$, respectively):

$$\frac{1}{\rho}\partial_z \tau_x = -f\beta_{ek}\left[\tau_x \sin(\theta_{ek}) + \tau_y \cos(\theta_{ek})\right] \quad (2)$$

2.4 Statistical methods and diagnostics

All diagnoses in this study will be borne out through the computation of mean square (MS) values over colocations. The MS of variable x is denoted by its capital letter, e.g. $\langle x^2 \rangle = X$ (for example $\langle \epsilon^2 \rangle = \mathcal{E}$, $\langle a_i^2 \rangle = A_i$ etc). All terms on the left-hand side of (1) are denoted as a_i-terms in this section. MSs and variances can be used without distinction in this analysis, because mean values are smaller than 2% of their standard deviations.

Summing the a_i-terms according to equation(1), they will partially balanced each other out, leaving a residual that contains unbalanced errors. A first way to quantify closure over the colocation dataset is thus to estimate the MS of this residual :

$$\mathcal{E} = \langle (\sum_i a_i)^2 \rangle. \quad (3)$$

While reconstructing the momentum balance, the sum of the MSs of the a_i-terms, that we denote Σ, is decomposed into two components : a balanced signal component β, that is closely related to the momentum signal that is effectively canceled in the momentum conservation reconstruction, and the residual MS $\mathcal{E}$ that contained the errors preventing a perfect closure. These quantities are related through:

$$\sum_i A_i = \underbrace{\Sigma}_{\text{Total sum of the } a_i\text{-term MSs}} = \underbrace{\beta}_{\text{Balanced component}} + \underbrace{\mathcal{E}}_{\text{Residual MS}}. \quad (4)$$

If closure is extremely poor, i.e. if the a_i-terms do not balance out at all, then the residual MS equals Σ. The sum Σ is thus used to define as second way to quantify closure, the degree of closure β/Σ, that compares the portion of MS in the balanced signal component relative to Σ.

Then, the balanced signal component can also be decomposed in terms of paired contributions X_{ij}, that represent the portion of the balanced signal component that is explained by the equilibrium between two individual terms a_i and a_j :

$$\beta = \sum_{i,j\neq i} X_{i,j} \text{ with } X_{i,j} = -2\langle a_i a_j \rangle, \quad (5)$$

with $\langle a_i a_j \rangle$ the covariance between the a_i-terms a_i, a_j.

Finally, the balanced signal component and residual MS are rewritten on a per-term basis to highlight their origins:

$$\beta = \textstyle\sum_i \beta_i \quad (6)$$
$$\mathcal{E} = \textstyle\sum_i \mathcal{E}_i \quad (7)$$

with:

$$\begin{cases} \beta_i = \dfrac{1}{2}[A_i + (\mathcal{E}_{-i} - \mathcal{E})] = -\displaystyle\sum_{j\neq i} \langle a_i a_j \rangle = -\langle a_i \epsilon_{-i} \rangle \\ \mathcal{E}_i = \dfrac{1}{2}[A_i - (\mathcal{E}_{-i} - \mathcal{E})] = \langle a_i \epsilon \rangle \end{cases} \quad (8)$$

where $\mathcal{E}_{-i}$ is the residual MS of a reconstruction without introducing the a_i-term. As shown by equation(8), the more an a_i-term reduces the residual MS via the difference

$\mathcal{E}_{-i} - \mathcal{E}$, the higher its contribution to momentum conservation β_i is and the lower its residual contribution $\mathcal{E}_i$ is. Alternatively, the balanced signal contribution of a term to momentum conservation β_i can be understood as the opposite of the sum of its covariances with the other terms and its residual contribution $\mathcal{E}_i$ as its covariance with the residual.

However, the meanings of β_i and $\mathcal{E}_i$ are clear in the particular case in which each term of the momentum conservation a_i can be decomposed into a balanced physical signal and an error that is uncorrelated with all other errors or balanced signals, giving

$$\underset{\substack{\text{Total}\\\text{signal}}}{a_i} = \underset{\substack{\text{Balanced}\\\text{physical signal}}}{b_i} + \underset{\text{Error}}{e_i} \tag{9}$$

with

$$\sum_i b_i = 0 \text{ and } \sum_i e_i = \epsilon. \tag{10}$$

In this particular case, one can show that contributions β_i and $\mathcal{E}_i$ are equal to the MSs of the contributions of the balanced physical signals and their errors:

$$\beta_i = B_i = -\sum_{i \neq j} \langle b_i b_j \rangle \text{ and } \mathcal{E}_i = E_i. \tag{11}$$

In the more general case, the interpretation of β_i and $\mathcal{E}_i$ as the contributions of balanced physical signals and their errors is approximate due to residual correlations between error and physical signals. The accuracy of this terminology for our reconstructions and the impact of these correlations can be quantified by closely examining the nature of the different sources of errors that lead to misclosure. We identify these errors as follows:

1. Resolution mismatch errors: some physical signal in one term, say a_i, remains unbalanced by other terms because of their lower spatial and/or temporal resolutions. This unbalanced variance will be contained in the residual contribution $\mathcal{E}_i$ associated with a_i, i.e. the most highly resolved term.
2. Missing physics: some physical signal in one term, say a_i, remains unbalanced because the term that should provide the balancing signal is simply absent from the reconstruction (Equation 1). In the present study, such errors can be related to baroclinic pressure gradients, vertical advection or horizontal dissipation.
3. Instrumental errors: typically due to noise on drifter position or on altimetric sea level measurements.
4. Physical modeling errors: for example resulting from inaccurate representation of the vertical stress divergence (Ekman dynamics and its parametrization).
5. Colocation errors: terms in Equation 1 are not estimated at the same position and time, but with spatial and temporal mismatches of up to 25 km and 30 min, respectively.

Resolution mismatch and missing physics errors are not correlated to other terms' physical signal or error components, because they by definition represent physical signals that are unbalanced by the other terms. Instrumental errors such as noise on altimetric or drifter measurements are reasonably approximated as uncorrelated (Spydell et al., 2019; Dufau et al., 2016) in which case they are not correlated to both physical signal or other errors. Lagrangian and Coriolis accelerations come of course from the same drifter measurements, but also come from orthogonal directions, and related instrumental errors can thus be considered as uncorrelated as well. Physical modeling errors are suspected for the wind term. To investigate its importance we quantify the effect of a scaling error on the wind term by a factor α (see Text 2 of Supporting Information). Scaling factors of 0.5 and 1.5 on the wind term increases the residual MS only by about 1% and 4% of its value, respectively. This is an indication that modeling errors on the wind term have a limited impact on momentum balance reconstructions. The four previous error sources are thus expected to produce balanced signal contributions that are of physical origin. This is not the case for colocation errors (Text 2 of Supporting Information). These errors indeed affect both the residual and balanced contributions with mirrored effects : the residual contribution of a term increases as much as its balanced signal contribution decreases compared with the no-colocation-error case (see Supporting Information Text 2 for the complete description). These colocation errors can be estimated through their dependency to the colocation mismatch as done in Section 3.2.1. They represent a consequent part of the residual contributions and so will be taken into account in the error budget of Section 3.2.1 along with the other errors. However, they are found to be small compared with the corresponding balanced signal contributions (representing at most 7% of the balanced signal contribution for the pressure gradient term). The balanced signal contributions is thus quasi entirely of physical origin. This finally justifies the physical meaning we accord to these balanced signal contributions.

For clarity, we introduce the unit γ, which is equal to the acceleration related to a dynamic sea level gradient of 1 mm per km. Thus, γ equals 9.81×10^{-6} m.s^{-2}. For global results, the 95% confidence intervals on the different metrics are computed assuming Gaussianity for the distribution of the means and using the central limit theorem. For binned results, a bootstrap method was applied with 9999 resamplings (Efron & Tibshirani, 1994).

2.5 Global vs. geographical analyses

The metrics introduced in Section 2.4 were first the subject of a global computation as presented in Section 3.1. Then, to highlight regional variability, the same metrics were also computed in 5°-geographical bins. Binned estimations are subject to more substantial relative statistical error for bins with lower numbers of colocations (Figure S2 in Supporting Information). Geographical bins in which these relative errors are higher than 50% are not shown. The mean number of colocations per 5°-bin was about 160 (distribution plotted in the inset of Figure 1).

3 Results and discussion

3.1 Global average diagnoses

The pressure gradient and Coriolis acceleration terms are largest for global averages, representing together 86% of the sum of MSs (Figure 2). This is expected from the dominance of sub-inertial motions on ocean surface variability (Yu, Garabato, et al., 2019; Arbic et al., 2022) and the validity of geostrophy for this class of motions. The Lagrangian acceleration and wind terms are weaker, representing 12% and 2% of the sum of MSs, respectively.

The closure of momentum balances reconstructed with along-track sea level data is measured by the global-scale average residual MS, which is $(1.64 \pm 0.03)\ \gamma^2$. This value corresponds to a degree of closure of about (80.5 ± 0.4)%. This high degree of closure translates into a large majority of individual MSs being balanced (see balanced signal vs. residual contributions in Figure 2a second bar chart).

When considering the drifter-matchup AVISO reconstruction, the global average residual MS was $(1.27\pm0.02)\ \gamma^2$, with an associated closure degree of (81.9 ± 0.4)% (Figure 2b). The residual MS is thus reduced by about 20% with AVISO data. Using AVISO data rather than along-track altimetry has two counter balancing effects on the residual MS. On one hand, the smoothing of altimetric information in AVISO data prevents from explaining small scale variability contained in the terms estimated from drifter data. Resolution mismatch errors are introduced in other words. This is shown by the smaller pressure gradient balanced signal contribution with AVISO data (2.08 $\pm$ 0.04) γ^2 compared with (2.57 $\pm$ 0.04) γ^2 with the along-track sea level data (Figure 2 second line). On the other hand, the residual MS is reduced by the combination of the same smoothing which partially deletes pressure gradient term instrumental errors and the estimation of the pressure gradient at the drifter-matchup which deletes colocation errors. This is demonstrated by the quasi absence of residual contribution in the pressure gradient term, unlike that of the along-track sea level data (9%). The improved performance of drifter-matchup AVISO reconstruction in terms of residual MS suggests that AVISO mapping deletes more instrumental errors and colocation errors than it introduces resolution mismatch errors. Interestingly, the larger amount of balanced information in along-track sea level data compared to AVISO helps increase the contribution of the balanced component in drifter observations: the Lagrangian acceleration balanced signal contribution is (0.83 $\pm$ 0.03) γ^2 compared with (0.62 $\pm$ 0.02) γ^2 for AVISO data and the Coriolis acceleration balanced signal contribution is (3.20 $\pm$ 0.05) γ^2 compared with (2.91 $\pm$ 0.04) γ^2 using AVISO data (Figure 2a and b second lines). The processes resolved by along-track and drifter trajectories explaining these differences are likely high-frequency and/or submesoscale features that have been filtered out by AVISO mapping process. This result highlights the additional value of along-track altimetry in accounting for fine scales and providing more complete momentum balance reconstructions.

Using along-track reconstruction, the global dominant dynamical pair is, as expected, the geostrophic pair (contribution of (4.77$\pm$ 0.09) γ^2 so 57% of Σ) (Figure 2a). The second and third most important pairs are the Lagrangian and Coriolis accelerations pair (1.19$\pm$ 0.03) γ^2 or 14% of Σ) and the Lagrangian acceleration and pressure gradient pair (0.49$\pm$ 0.03) γ^2 or 6% of Σ). Note that three-term balances such as cyclogeostrophy or those involved with gravity waves likely contribute to the diagnoses of these pairs, but three-term balances are beyond the scope of the present analysis. The Coriolis acceleration and wind term paired contribution, i.e. Ekman-like dynamics, accounts for (0.43$\pm$ 0.01) γ^2 or 5% of Σ. Contributions from the last two dynamical pairs, the Lagrangian acceleration-wind and pressure gradient-wind term pairs, are of smaller amplitude and negative. These negative values may indicate that the two terms in the pairs tend to increase or decrease together and thus must balance out together with a third term. Using the drifter-matchup AVISO reconstruction instead of the along-track reconstruction reduces the geostrophic contribution (4.2 $\pm$ 0.07) γ^2 and the contribution of the Lagrangian acceleration-pressure gradient term pair (0.07 $\pm$ 0.02) γ^2, highlighting once again that AVISO cannot render small-scale variability. Regardless of the altimetric data (e.g. along-track or AVISO), about 28-30% of the total balanced signal variance is explained by ageostrophic motions, which can therefore not be ignored for accurate reconstruction of surface momentum balance.

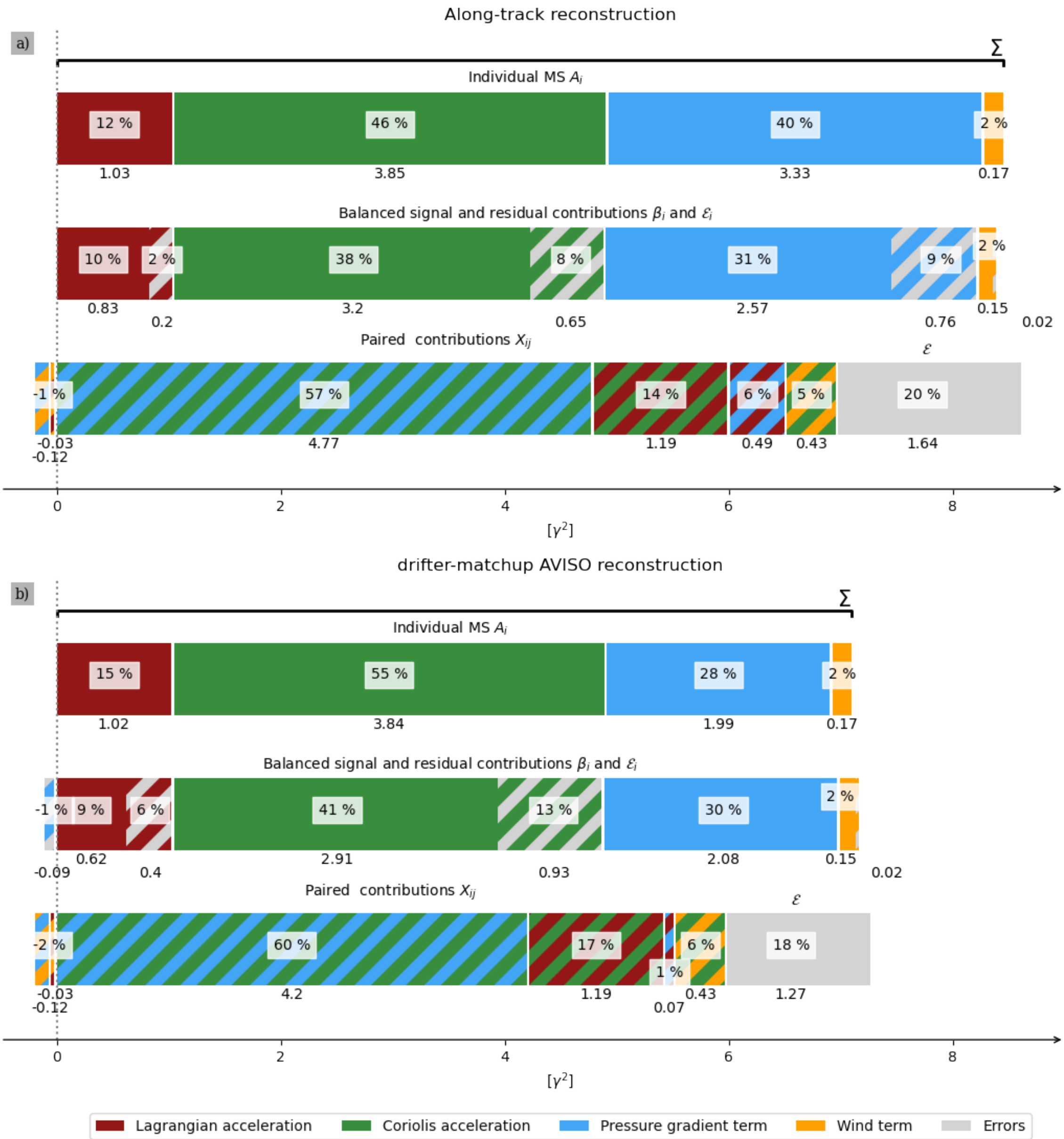

Figure 2. Dashboards of momentum closure decompositions using along-track reconstruction (a) and drifter-matchup AVISO reconstruction (b) (see Section 2.4, Equations 4, 5-7). The top horizontal bar charts show the MSs from each term. Middle bar charts are the decomposition into balanced signal and residual contributions for each term. Bottom bar charts show the decomposition into paired contributions (pairs are indicated by the two-color hatching) and the final residual MS. Each bar is annotated with the corresponding percentage of Σ (total top bar chart) and the corresponding MS expressed in γ^2. Negative quantities are moved towards negative abscissas.

3.2 Exploring misclosure

We now attempt to characterize and quantify the importance of the different sources of errors enumerated in Section 2.4 that lead to the observed misclosure.

3.2.1 Colocation errors

The temporal mismatch criterion ΔT <30 min is small compared with characteristic timescales of dominant surface processes (typically $\leq$ 12 h) and temporal mismatches are thus not expected to lead to substantial temporal colocation errors. This assumption is confirmed by the lack of dependency of momentum closure on temporal mismatches (Figure S1 in Supplementary Information).

We thus surmise that colocation errors are dominated by spatial mismatches. The sensitivity of closure to spatial mismatch is provided by averaged residuals conditioned by spatial mismatch in bins of 2 km width. For this section and this section only, colocations with spatial mismatches up to 200 km were considered. The mean number of colocations per 2 km bin was 19,268, with the distribution being almost uniform.

Along-track and altimeter-matchup AVISO momentum residual MSs steadily increase as a function of spatial mismatch, reaching values 3.6 and 2.7 times their respective minimum values, for mismatches of 100 km (Figure 3a). This increase slows for larger mismatches, indicating that the spatial scales of energetic motions that mainly contribute to momentum balance here are of around 100 km or more (e.g. mesoscales). Ultimately, the pressure gradient is expected to become fully uncorrelated with other terms and the residual MS should converge to $\mathcal{E}_{-g\partial_x\eta}+A_{g\partial_x\eta}$ (max. lines on Figure 3a). This dissociation does not appear to have occurred at scales under 200 km. The increase of residual MS with spatial mismatch translates into a transfer from balanced signal component to residual contribution for all terms except the wind term (Figure 3c and d).

The difference in residual MSs between along-track and altimeter-matchup AVISO increases with spatial mismatch and plateaus at about 100 km (visible on the difference of residual MSs, not shown) to a value that is comparable to the difference in pressure gradient MSs (Figure 3a). The faster increase of the along-track residual reflects the signature of processes that are present in along-track data, but not in AVISO data, presumably due to their finer spatial scales. This pattern is also apparent for the Coriolis-pressure gradient pair contribution from the altimeter-matchup AVISO reconstruction, which becomes comparable to the along-track reconstruction at scales of about 100 km also (Figure 3b).

The drifter-matchup AVISO momentum residual also increases with spatial mismatch, but to much lesser extent (reaching only 1.1 of its value at minimal mismatch at 100 km). The AVISO pressure gradient was interpolated at the exact drifter position and time; therefore, there are no colocation errors, strictly speaking. These errors are rather related to AVISO mapping process, which builds a gridded product from the optimal interpolation of distant along-track altimetric data. These errors are negligible compared to others and thus will not be further discussed.

To estimate the amplitude of colocation errors on the global average residual MSs, the residual MS for spatial mismatch below 4 km (red lines on Figure 3a inset axes) is substracted from the global $[0, 25\text{km}]$ averaged residual MS presented in Section 3.1. The resulting along-track total colocation error is about 0.35 γ^2, i.e. 21% of the corresponding global residual MS.

The sensitivity of the residual MS to spatial mismatch (Figure 3a) can be decomposed as the sum of individual residual contributions sensitivities (Figure 3b). This decomposition is dominated by the Coriolis and pressure gradient residual contributions, whose sensitivities therefore closely resemble residual sensitivities. The Lagrangian term

Table 1. Error budget for along-track reconstruction: MSs, balanced signal and residual contributions and errors for both individual and total values

	Lagrangian acceleration	Coriolis acceleration	Pressure gradient	Wind term	Total
MS	1.03	3.85	3.33	0.17	$\Sigma = 8.38$
Balanced signal contribution $[\gamma^2]$	0.83	3.20	2.57	0.15	6.75
Residual contribution $[\gamma^2]$	0.20	0.65	0.76	0.02	$\mathcal{E} = 1.64$
Colocation error					
$[\gamma^2]$	0.02	0.14	0.19	negligible	0.35
[% of residual]	1.2%	4.9%	12%	negligible	21%
Resolution mismatch error					
$[\gamma^2]$	0.18	0.51	-	-	0.69
[% of residual]	11%	31%	-	-	42%
Instrumental error					
$[\gamma^2]$	negligible	negligible	0.57	-	0.57
[% of residual]	negligible	negligible	36%	-	36%

error exhibits some sensitivity for the along-track sea level reconstruction, but no clear sensitivity for the altimeter-matchup AVISO reconstruction. This is consistent with the weak balance between Lagrangian and pressure gradient terms in the AVISO reconstruction (Section 3.1, Figure 2, Figure 3b). The wind term error did not show any clear sensitivity to spatial mismatch over the values considered (≤ 200 km). This insensitivity likely stems from the negligible correlation of the wind term with the pressure gradient term (Section 3.1).

Applying the same method as for the estimation of total colocation error, individual colocation errors were estimated by subtracting the residual contributions for spatial mismatch below 4 km from $[0, 25\text{km}]$ averaged values (Table 1). These colocation errors echo the discussion above on residual contribution sensitivities on spatial mismatch and will be useful for estimating resolution mismatch errors as well as instrumental errors.

The contributions of the Lagrangian-Coriolis accelerations and Ekman (Coriolis acceleration-wind) pairs to momentum balance closure are insensitive to spatial mismatch, as expected because both terms are estimated at the drifter-matchup point. The geostrophic pair dominates by a factor of 4 over the Lagrangian-Coriolis pair at small spatial mismatches for along-track reconstruction, consistently with the individual term decomposition (Figure 3 b). The geostrophic pair decreases with spatial mismatch and contributes less than the Lagrangian-Coriolis accelerations pair for spatial mismatches larger than 150 km. An exponential fit on this decrease leads to decay length scales of about 91 ± 5 km for along-track sea level reconstruction and 119 ± 9 km for altimeter-matchup AVISO reconstruction. This finding emphasizes the dominance of mesoscale motions on momentum balance closure. The difference in decay scale, the larger balanced signal contributions at minimal spatial mismatches with along-track data, and the merging of along-track and AVISO contributions at lags smaller than about 100 km all suggest that finer scale variability is captured with along-track data as argued above. The Lagrangian acceleration-pressure gradient pair contributes at most to about half of the Lagrangian-Coriolis pair for along-track data and smallest spatial mismatch. An exponential fit on the Lagrangian acceleration-pressure gradient pair sensitivity gives a decay length scale of 43 ± 4 km, indicating a reduced spatial scale of the processes contributing to the momentum balance via the Lagrangian acceleration-pressure gradient balance compared with the geostrophic balance. With altimeter-matchup AVISO data, the Lagrangian acceleration-pressure gradient pair contributes much more weakly to momentum balance (factor of $\sim$6 compared with along-track data), but shows some decay at a comparable length scale. At spatial mismatch larger than about 100 km, along-track and altimeter-matchup AVISO data lead to comparable balanced signal contributions (see also Figure 3d), and AVISO data may be more useful given its lower noise level.

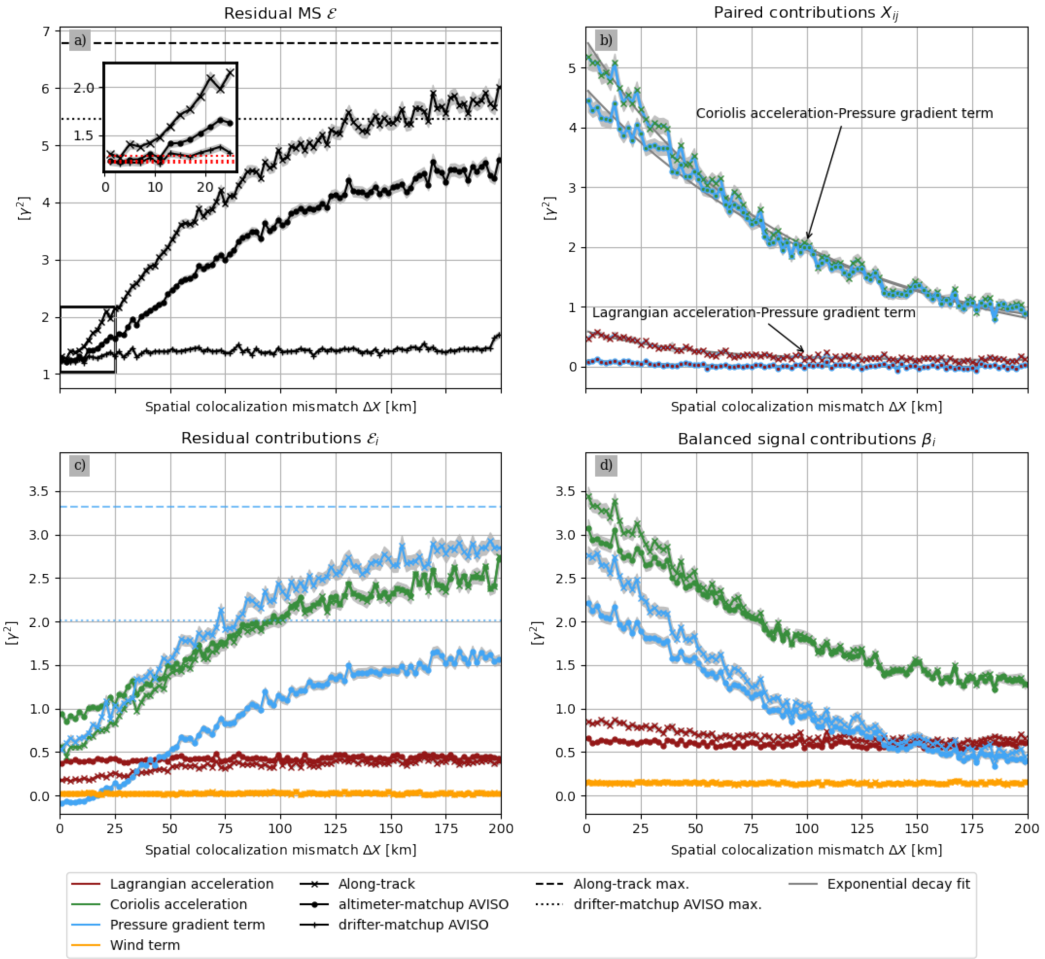

Figure 3. a) Residual dependency on spatial colocation mismatch for the three different reconstructions (along-track, drifter-matchup AVISO and altimeter-matchup AVISO). The ultimate maximum values $\mathcal{E}_{-g\partial_x\eta} + A_{g\partial_x\eta}$ where the pressure gradient term would be fully uncorrelated are plotted as horizontal lines. Red lines on the inset highlight values for spatial colocation mismatches of less than 4 km used to estimate global colocation errors. b) Dependency on spatial colocation mismatch of the contribution of the Coriolis acceleration-pressure gradient term pair and the Lagrangian acceleration-pressure gradient term pair. The exponential decay fit is also plotted. c) and d) are respectively the dependency of the balanced signal and the residual contributions on spatial mismatch. Horizontal lines are the ultimate maximums for the pressure gradient residual contribution for along-track altimetry and altimeter-matchup AVISO reconstructions. Diagnoses were averaged over colocations in 2 km spatial mismatch bins. The 95% confidence intervals are plotted in gray.

3.2.2 Resolution mismatch errors

Given the high temporal resolution and local footprint of drifter observations compared with sea level and wind sources, we expect Lagrangian and Coriolis accelerations to contain large resolution mismatch errors. Assuming both of these terms are devoid of instrumental noise (Appendix A1), subtracting the previously estimated respective colocation errors (Section 3.2.1 and Table 1) in the Lagrangian and Coriolis acceleration errors components leads to estimates of resolution mismatch errors of about 0.18 γ^2 and 0.51 γ^2, respectively (Table 1). We then explored whether these variances can be explained by unmeasured pressure gradient or wind terms. Altimetric sea level observations are smoothed with a 65 km low pass filter that removes all finer scale variability (Quality Information Document of the along-track product). Assuming the missing pressure gradient variance is the sum of Lagrangian and Coriolis acceleration mismatch errors ($\epsilon_r =$ 0.18 γ^2+0.51 γ^2= 0.69 γ^2) and that signals missed in altimetric data are characterized by a spatial scale L of 65 km, a rough estimation of the corresponding sea level standard deviation is $\sqrt{\epsilon_r}\gamma \times L/g \sim 5$ cm. This estimated standard deviation being a fraction of the total sea level variability, we conclude that missing information in altimetric sea level may explain the resolution mismatch errors derived above. Having no knowledge on the information missing in wind reanalysis or on the quality of the physical model employed to estimate vertical stress divergence, we cannot provide meaningful estimates of associated errors at this stage.

In principle, the pressure gradient can also contain resolution mismatch error if correlated information is missing in the wind term. In the present state, there is little correlation between the pressure gradient and the wind term (Figure 2). In the literature, Bonjean and Lagerloef (2002)'s diagnostic model shows that equatorial surface dynamics can be simplified to the pressure-gradient-compensating wind term, potentially resulting in resolution mismatch errors in our study. However, this would be relevant only for a small proportion of the colocations; furthermore, we are not aware of other global observations or dynamical expectations regarding a systematic correlation between the pressure gradient and wind terms at the ocean surface. Moreover, the drifter-matchup AVISO pressure gradient term exhibits negligible errors compared with the balanced signal component, thereby voiding the possibility of such resolution mismatch error for AVISO data (Figure 2b). We therefore conclude that resolution mismatch errors between the pressure gradient and wind terms are unlikely to have a strong signature on the global residual.

3.2.3 Instrumental errors

Drifter position data errors provided with the GDP dataset have a median of 60 m and 400 m for GPS and Argos drifters, respectively, and have repercussions on velocity and acceleration data. As shown in Appendix A1, most of these drifter instrumental errors in Coriolis and Lagrangian accelerations residual contributions are effectively removed from the studied residual by the LOWESS method (Elipot et al., 2016) and the temporal 2.5 cpd low-pass filter.

For the pressure gradient, the processing that lead to along-track and AVISO sea level products mitigates instrumental noise via spatial low-pass filtering (65 km cutoff) and optimal interpolation, respectively (Quality Information Document of the along-track product). The pressure gradient term estimated from AVISO data is fully balanced out by other terms (Figure 2). AVISO instrumental noise is therefore necessarily negligible.

For the along-track reconstruction, after removing the colocation errors quantified in Section 3.2.1, about 0.57 $\gamma^2$of the pressure gradient residual contribution are still to be accounted for. The resolution mismatch error in the pressure gradient term is expected to be small as argued in Section 3.2.2. By process of elimination, instrumental noise in the pressure gradient term residual contribution must thus represent up to 0.57 γ^2, which is also 36% of the residual MS. For the along-track product used, the remaining sea level error after the 65 km low-pass filtering is reported to lie between 0.85 and 1.1 cm, depending on the altimeter considered (Quality Information Document of the along-track product). Assuming this error is spectrally white up to wavelengths δ_x of 65 km with a variance ϵ_η of 1 cm, the error on the pressure gradient term is $(g\epsilon_\eta \times 2\pi/\delta_x)^2/3 \sim 0.3\,\gamma^2$. This is a loose confirmation that the remaining error on the pressure gradient may be explained by intrumental noise. Going further would require a more detailed analysis of the along-track altimetric noise spectral distribution and processing, its projection on the present diagnostics which fall outside of the scope of the present work.

3.2.4 Missing physics errors

Finally, our reconstruction of near-surface momentum balance neglects several physical processes contributions including, for instance, the baroclinic pressure contribution associated with horizontal density gradients $\partial_x \rho$. According to Fox-Kemper et al. (2011), such density horizontal gradient variance $\langle \nabla \rho^2 \rangle$ can reach maximum values of up to 3×10^{-10} kg^2.m^{-8} in simulations of the Southern Ocean. The error induced on momentum at depth scales h of 15 m is $(gh/\rho_0)^2 \times \langle \nabla \rho^2 \rangle = 0.006\,\gamma^2$, which is a small fraction (about 0.4%) of the residual. Vertical advection of the horizontal momentum is neglected on the basis of the weakness of vertical velocity near the ocean surface. The estimation of the horizontal turbulence contribution is complicated here by the isolated nature of drifter observations, which do not provide meaningful grounds for scale separation. In conclusion, in this study, we assumed that missing physics errors are small compared with the other error sources.

3.3 Geographical analysis

3.3.1 Momentum balance closure

We now turn away from the global-scale average diagnoses to describe how momentum balance varies regionally. In an absolute sense, closure is best in the equatorial zone and in moderately energetic regions such as oceanic gyre centers (Figure 4a). At mid to high latitudes and/or in energetic areas, momentum balances closure is lower, with residual MSs typically exceeding the global average ($1.64\,\gamma^2$). A potential explanation involves decreased values of energy-dominant spatial scales at these latitudes as indicated by observed eddy sizes in Chelton et al. (2011), which fall below 75 km at latitudes polewards of 45°. This shortening of the scales of variability can increase the amount of unresolved variability in altimetric data, thereby increasing resolution mismatch error on Coriolis acceleration. This difference in variability scales would also increase colocation errors. Both trends are consistent with the larger values of Coriolis acceleration and pressure gradient residual contributions (Figures 4c and 4d). Furthermore, the larger increase in Coriolis acceleration residual contributions compared with those of the pressure gradient may indicate that resolution mismatch errors weigh more than colocation errors on the residuals in these areas. In the Aghulas, Gulf Stream, and Kuroshio current systems, the residual is driven by pressure gradient term contribution (Figure 4d). As geostrophy is the main contributing equilibrium in these areas, colocation errors in the residual contributions of the pressure gradient term and of the Coriolis acceleration should be of the same order of magnitude. Given the more modest Coriolis residual contribution, the pressure gradient residual contribution observed in this areas is thus unlikely to result from colocation errors (Figures 4c and 4d). Resolution mismatch errors associated with the wind term are also unlikely, because winds are not particularly strong there. These errors thus appear to reflect an increase in altimetric instrumental errors, which may potentially be related to the surface wave field via the heterogeneities induced by its interactions with ocean circulation (Quilfen et al., 2022).

3.3.2 Dynamical regimes

We identified characteristic dynamical regimes in selected regions (contours on Figure 4a). These regions were chosen for the contrasting nature of their momentum balance closures, as indicated by dynamical paired contributions and a priori dynamics (e.g. expected strong geostrophy in the Gulf Stream etc (Yu et al., 2021)). The Gulf Stream region (GS) is defined by locations between 15°N and 50°N and 85°W and 0°W where the geostrophic pair contribution is greater than 70%. The Antarctic Circumpolar Current region (ACC) is composed of locations southwards of 35°S, where the geostrophic pair contribution is greater than 40%. The North Pacific region (NP) is the region extending from 120°E to 150°W and northwards of 40°N where the Lagrangian acceleration - Coriolis acceleration pair contribution exceeds 10%. This definition thus excludes the Kuroshio Current. Finally, the Equator region (EQ) is defined as the area in between 15°S and 15°N.

In GS and ACC, geostrophy dominates the ocean surface dynamics, explaining about 80% of the momentum balance closure, compared with 57% for the global average (Figure 5a). Remarkably, the same percentage of geostrophic variance in these energetic regions was also estimated through the numerical reconstruction of Yu et al. (2021). The Lagrangian-Coriolis and Lagrangian-pressure gradient pairs contribute relatively less to the momentum closure compared with the global averages, emphasizing the relatively moderate amplitude of cyclogeostrophic corrections, even in these energetic areas. In ACC, the pressure gradient-wind terms pair is barely higher than the global average in relative terms (7% vs. 5%), but twice as high in absolute values, which is consistent with our expectations of strong winds in this region.

In NP, the dominant dynamical equilibrium is that associated with the Lagrangian-Coriolis pair (41%, Figure 5c), reflecting the higher near-inertial variability in this region as reported in Yu, Ponte, et al. (2019); Liu et al. (2019); Flexas et al. (2019). The geostrophic pair (30%) is of secondary importance. Internal tides may also contribute to the balance via the combinations with these pairs.

The momentum balance observed in EQ is in stark contrast with those in all other regions, with the dominance of the Lagrangian-pressure gradient pair (30% of the closure, Figure 5d). Internal tides are energetic in this area (Buijsman et al., 2017) and may contribute to momentum balance via the Lagrangian-Coriolis and Lagrangian-pressure gradient pairs. The modest contribution of the pressure gradient-wind term pair and the absence of correlations with pressure gradient terms (expected from Bonjean and Lagerloef (2002)) may most likely be explained by the poor estimation of the wind term. These poor estimates may arise due to the use of global Ekman parameters and the pronounced variations of these parameters away from global averages at near equatorial latitudes (Rio et al., 2014). Given the lower noise level in altimetric data near the equator (Figure 4d), our inability to close momentum balances there may therefore be driven by this poor estimation of the wind term.

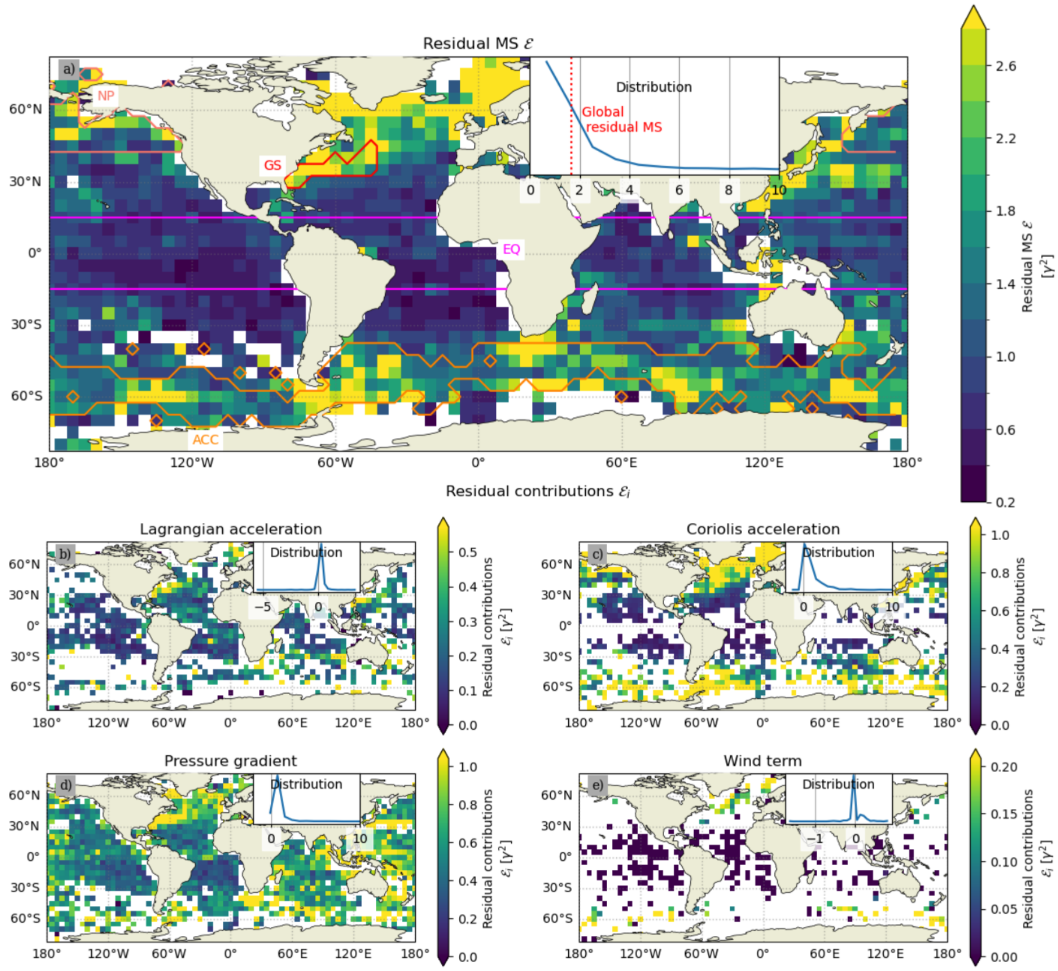

Figure 4. The residual mean square value (a) and residual contribution of Lagrangian acceleration (b), Coriolis acceleration (c), pressure gradient (d) and wind (e) terms mapped in 5°-geographical bins. Only bins in which the relative statistical errors are less than 50% are shown. Contours in a) delimit the different dynamical regimes in Figure 5. Note that the color bar scales differ between graphs.

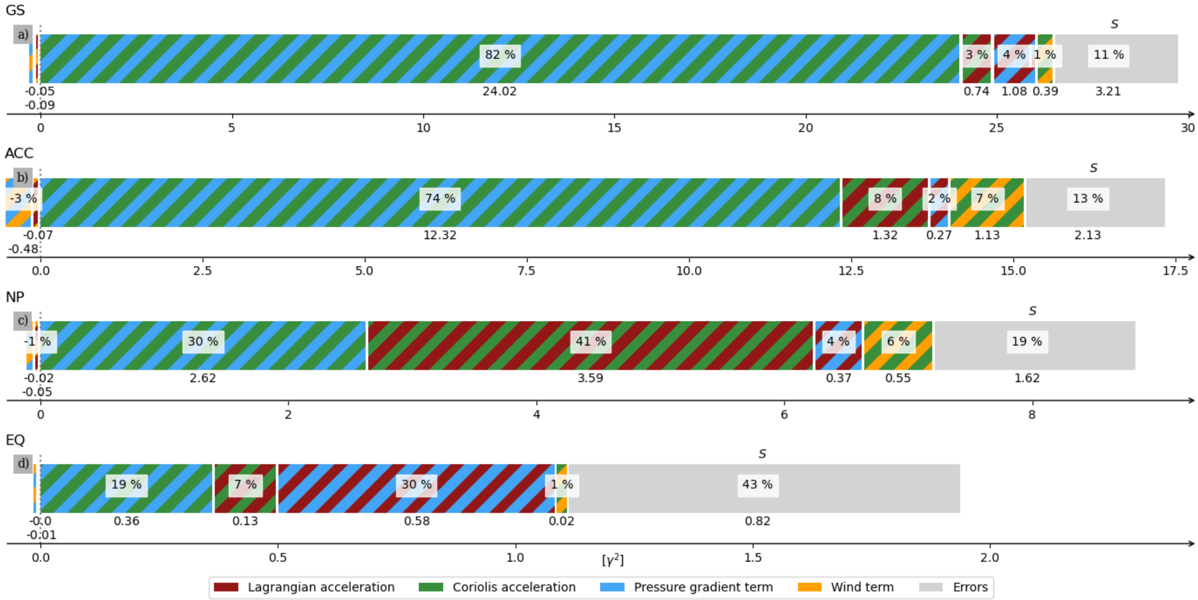

Figure 5. Different decompositions of paired contributions for areas plotted on Figure 4a i.e. the Gulf Stream (GS), the Antarctic Circumpolar Current (ACC), the North Pacific (NP) and the Equatorial Band (EQ). Note the differences between the horizontal axes.

4 Conclusion

By combining current and sea level observations and wind reanalysis, we successfully reconstructed global instantaneous near-surface horizontal momentum balances at a 80% closure degree (β/Σ). This success motivated the investigation of dominant terms and dynamical equilibria, and geographic sensitivities. As expected, geostrophy is the leading order equilibrium, explaining about two thirds of the variance in the balanced signals at a global scale. In western boundary current systems and ACC, geostrophy dominates and explains up to 81% and 91% of the balanced signal variance, respectively. However, our results also highlight that about one third of the ocean surface dynamics resolved here is not geostrophic. As reported by Yu et al. (2021), Lagrangian and Ekman flows thus cannot be neglected everywhere when reconstructing instantaneous near-surface balances. Geostrophy explains only one third of the balanced signal variance in the North Pacific (NP) and the equatorial band (EQ), for instance. We clearly demonstrated this specificity using observationally based quantitative information.

Gridded AVISO sea level reconstructions provide global resdiual MSs that are about 20% lower than with along-track sea level. This difference suggests that AVISO mapping deletes more instrumental errors than it introduces resolution mismatch errors. In addition, the novel methodology introduced here reveals that along-track altimetry presumably contains the signature of short-scale variability that is not present in AVISO and balances out better with the variability contained in drifter observations. Along-track altimetry effectively enables the compensation of Lagrangian acceleration by the pressure gradient that AVISO cannot.

We detailed the quantitative error budget for global closures using along-track sea level data. Colocation mismatch errors (between drifter and altimetric observations) are mainly spatial, and account for 21% of the global residual MS. Short-scale variability contained in drifter observations, but not in other data sources (altimetry, wind) results in a resolution mismatch errors that we estimate to be about 42%. Instrumental errors on sea level observations likely account for 36% of the residual. The remaining 1% are wind term errors, that are driven either by the quality of the wind reanalysis or by the accuracy of the Ekman model.

One limitation of our analysis stems from the quality of the Ekman model used for the estimation of the wind term. The Ekman model used is indeed implemented with global values of its parameters and therefore neglects the seasonal and regional variability reported in Rio et al. (2014). Departures from global parameter values are especially large at the equator for the amplitude parameter; this can only have an adverse effect on momentum balance closure. These departures may for instance explain the reason why we are unable to observe the equatorial pressure gradient-wind term compensation modeled by Bonjean and Lagerloef (2002). Further research can explore the seasonal and regional sensitivities of Ekman parameters such as those computed in Rio et al. (2014). The estimation of the vertical stress divergence may also benefit from more complete Ekman models that use knowledge on the mixed layer depth (Mulet et al., 2021) and/or the wind time history (Lilly & Elipot, 2021). At present, we cannot directly quantify the role of ERA* product inaccuracies on momentum closure. In this analysis, we relied on ERA* being the best product available to estimate the wind term. A sensitivity analysis of different wind reanalyses would be an interesting undertaking. In the preliminary stages of the analysis, we compared ERA5 with ERA* with no significant differences in global momentum closure.

The spatial colocation mismatch criterion set to 25 km resulted from a compromise between the mitigation of colocation errors and statistical reliability. It is possible to adjust this criterion regionally to match the geographical and temporal (seasonal) distributions of ocean spatial scales. For example, higher mismatch values at the equator may be able to help account for larger spatial scales (Chelton et al., 2011). Adjusting this criterion however requires building prior knowledge on these distributions. An a posteriori consideration of the small sensitivity of residuals on temporal mismatch can allow increasing the temporal tolerance when assembling colocations. Relaxing the temporal tolerance should be done cautiously, because it can affect closure in areas where energetic high-frequency motions are present and may also introduce correlated colocations. The largest benefit of these refinements is expected to be for geographically bin-averaged diagnoses whose statistical reliability is currently limited by the amount of available colocations. Another benefit would be to improve the closure in global diagnoses.

For the global averages, we did not attempt to account for biases introduced by non-uniform geographical sampling (driven by joint drifter and altimeter availability), due to limited data availability. Our methodology cannot identify three term balances (e.g. cyclogeostrophy, internal tide dynamics); clustering approaches need to be developed to do so. Statistical diagnoses may have been conditioned on temporal (seasonal) criteria to highlight associated variability. Testing our momentum reconstruction methodology with numerical simulations of ocean circulation can help assess the above-cited limits and actual usefulness of the proposed improvements. In particular, the signature of specific dynamical processes (e.g. internal tides, near inertial waves) in simplified simulated cases can help identify such processes in reconstructions based on observational data.

With its unprecedented resolution and accuracy (Fu et al., 2024), the use of SWOT wide-swath sea level is expected to substantially reduce instrumental and resolution mismatch errors, and to considerably improve horizontal surface momentum balance reconstructions. The two-dimensional nature of SWOT sea level observations will make it possible to reconstruct momentum balance in both horizontal dimensions simultaneously. The wide-swath sea level data will also lead to a larger number of colocations and smaller, if not negligible, spatial colocation mismatch errors. The reconstructions of horizontal momentum balances and the methodology developed here should be instrumental to 1/ gain an observation-based understanding of the upper ocean dynamics, and 2/ assess the need to go beyond the framework employed to date to estimate the ocean circulation, namely geostrophy plus Ekman. This research effort can also contribute to validating SWOT sea level observations and to improving our ability to estimate MDT from these observations.

Appendix A Reconstruction sensitivity

Colocation datasets constructed as the one in Section 2.2, but considering a different drifter type, drogue status, and low-pass filter are built. Here, the sensitivity of closure to the low-pass filter cutoff frequency applied on drifter trajectories, the use of GPS or Argos positioning and drogued or undrogued drifters are studied using methods described in Section 2.4.

A1 Applying low-pass filters on drifter trajectories

We low-filtered drifter trajectories at different cutoff frequencies with a finite impulse response filter and applied forwards and backwards on drifter velocity. The combined filter thus has zero phase and a filter order twice that of the original.

Applying a 2.5 cpd low-pass filter on drifter trajectories reduces the residual contribution of the Lagrangian acceleration term by 0.84 γ^2(-44% of its MS), whereas the balanced signal contribution remains approximately constant (Figure A1a). This 2.5 cpd low-pass filter thus removed a substantial part of acceleration errors from drifter observations. GDP drifter instrumental velocity errors were estimated using the LOWESS smoothing method and directly available in the GDP dataset (Elipot et al., 2016). The mean velocity error is about $\epsilon_v = 2 \times 10^{-2}$m.s^{-1}, yielding approximate instrumental error variances of $(f\epsilon_v)^2 = 0.04\ \ \gamma^2$ for Coriolis acceleration and $\frac{\epsilon_v^2}{2dt^2} = 0.40\ \ \gamma^2$ for Lagrangian acceleration after centered finite differentiation. These errors are comparable to the amplitudes of the signal filtered out with the 2.5 cpd low-pass filter described above and corroborate the hypothesis that this information mostly represents instrumental position error. Differences between these two quantities can be explained by an imperfect velocity error estimation or by unbalanced resolution mismatch errors that are filtered out with instrumental errors. In any case, these results justify the use of low-pass filtering on drifter data for the global momentum balance reconstruction (Section 3.1).

Interestingly, decreasing the cutoff frequencies from 1.5 to 0.5 cpd progressively cancels the balanced signal contribution of Lagrangian acceleration and reduces that of Coriolis acceleration (Figure A1 a) and b)). This leads to a decrease in the balanced signal contributions of the other terms (Figure A1 c) and d)). These two filters thus hinder closure, but these experiments demonstrate that high-frequency processes, such as near inertial and tidal motions, are captured and do contribute to momentum balance closure.

A2 GPS vs. ARGOS

Despite their original difference in terms of positioning error (median of 60 m for GPS vs. 400 m for Argos), reconstruction with GPS or Argos drifters give similar results in terms of the balanced signal and residual contributions of the equation once filtered with 2.5 cpd low-pass filter (Figure A1e). This similarity justifies the use of both GPS and Argos drifters, making it possible to nearly double the number of available colocations.

A3 Drogued vs. undrogued

Undrogued drifters follows currents at the very surface and are more subject to wind drift than drogued drifters (Poulain et al., 2009). Therefore, the undrogued Coriolis acceleration MS is higher than the drogued one (+1.26 γ^2). This additional variability remains unbalanced in the reconstruction, and is thus added in the residual contribution of the Coriolis term (Figure A1f). This additional variability therefore justifies using only drogued drifters for our reconstruction analysis.

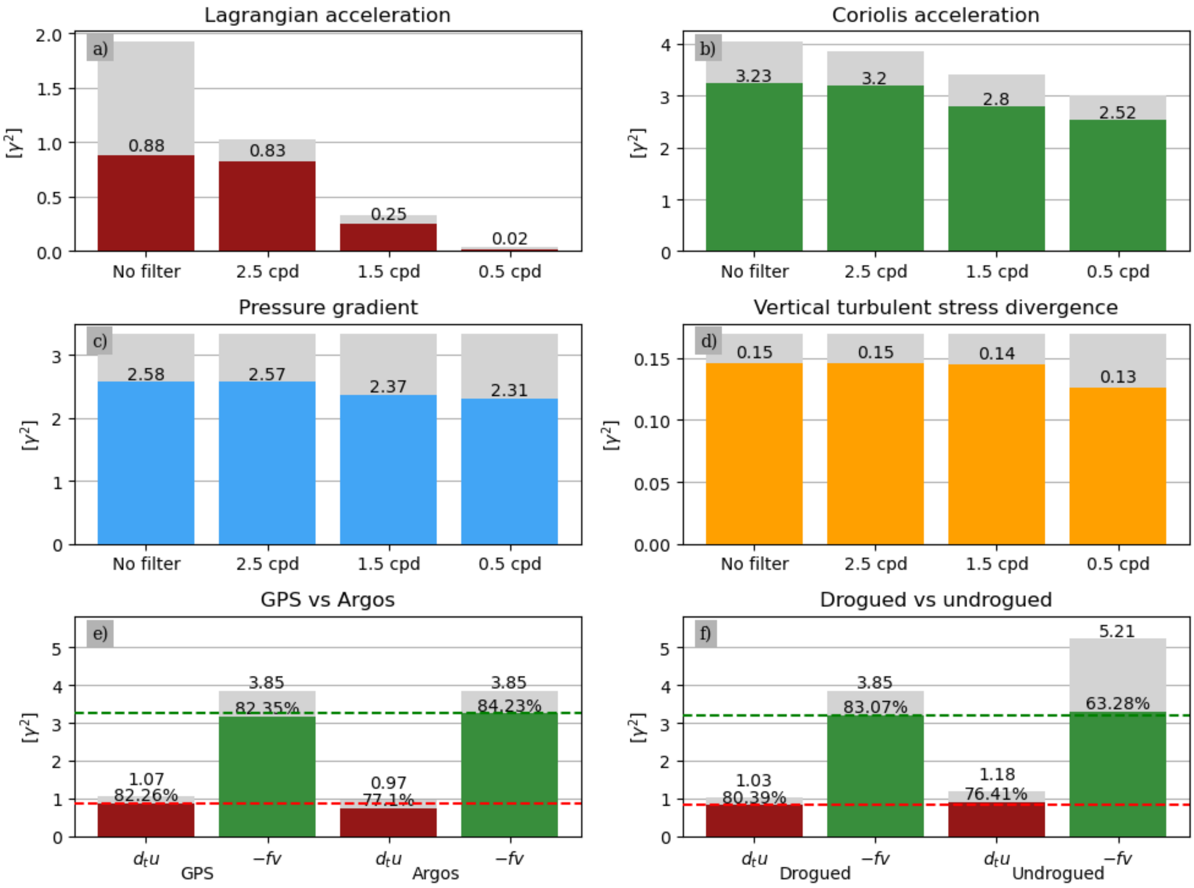

Figure A1. Decomposition into balanced physical signal (in color) and error (gray) components: (a to d) for all terms applying no filter or 2.5, 1.5 and 0.5 cpd-low pass filter on drifter trajectories; comparing the Lagrangian and Coriolis accelerations for drogued GPS and Argos drifters (e) and for drogued and undrogued drifters (f) with 2.5 cpd low-pass filtering

Open Research Section

Archived datasets used are available at the following references:

- for ERA* data : Trindade et al. (2022)
- for L3-along-track altimetry: European Union-Copernicus Marine Service (2021a)
- for L4-AVISO-gridded alitmetry: European Union-Copernicus Marine Service (2021b)

All codes and notebooks used are available in the dedicated repository: `https://doi.org/10.5281/zenodo.14513262` (Demol, 2024).

Acknowledgments
We thank Bertrand Chapron, Clément de Boyer Montégut and Yves Quilfen for insightful discussions that helped shape the present work. The study benefited from support by CNES via the TOSCA-ROSES SWOT project DIEGO.

References

Arbic, B. K., Elipot, S., Brasch, J. M., Menemenlis, D., Ponte, A. L., Shriver, J. F., ... Nelson, A. D. (2022). Near-Surface Oceanic Kinetic Energy Distributions From Drifter Observations and Numerical Models. *Journal of Geophysical Research: Oceans*, *127*(10), e2022JC018551. Retrieved 2023-12-07, from `https://onlinelibrary.wiley.com/doi/abs/10.1029/2022JC018551` (_eprint: https://onlinelibrary.wiley.com/doi/pdf/10.1029/2022JC018551) doi: 10.1029/2022JC018551

Ballarotta, M., Ubelmann, C., Pujol, M.-I., Taburet, G., Fournier, F., Legeais, J.-F., ... Picot, N. (2019). On the resolutions of ocean altimetry maps. *Ocean Science*, *15*.

Bonjean, F., & Lagerloef, G. S. E. (2002, October). Diagnostic Model and Analysis of the Surface Currents in the Tropical Pacific Ocean. *Journal of Physical Oceanography*, *32*(10), 2938–2954. Retrieved 2024-06-10, from `https://journals.ametsoc.org/view/journals/phoc/32/10/1520-0485_2002_032_2938_dmaaot_2.0.co_2.xml` (Publisher: American Meteorological Society Section: Journal of Physical Oceanography) doi: 10.1175/1520-0485(2002)032⟨2938:DMAAOT⟩2.0.CO;2

Buijsman, M. C., Arbic, B. K., Richman, J. G., Shriver, J. F., Wallcraft, A. J., & Zamudio, L. (2017). Semidiurnal internal tide incoherence in the equatorial Pacific. *Journal of Geophysical Research: Oceans*, *122*(7), 5286–5305. Retrieved 2024-06-10, from `https://onlinelibrary.wiley.com/doi/abs/10.1002/2016JC012590` (_eprint: https://onlinelibrary.wiley.com/doi/pdf/10.1002/2016JC012590) doi: 10.1002/2016JC012590

Chelton, D. B., Schlax, M. G., & Samelson, R. M. (2011, October). Global observations of nonlinear mesoscale eddies. *Progress in Oceanography*, *91*(2), 167–216. Retrieved 2024-06-07, from `https://www.sciencedirect.com/science/article/pii/S0079661111000036` doi: 10.1016/j.pocean.2011.01.002

Cronin, M. F., Gentemann, C. L., Edson, J., Ueki, I., Bourassa, M., Brown, S., ... Zhang, D. (2019). Air-Sea Fluxes With a Focus on Heat and Momentum. *Frontiers in Marine Science*, *6*. Retrieved 2023-12-06, from `https://www.frontiersin.org/articles/10.3389/fmars.2019.00430`

Davis, R. E., deSzoeke, R., Halpern, D., & Niiler, P. (1981, December). Variability in the upper ocean during MILE. Part I: The heat and momentum balances. *Deep Sea Research Part A. Oceanographic Research Papers*, *28*(12), 1427–1451. Retrieved 2023-12-20, from `https://www.sciencedirect.com/science/article/pii/0198014981900911` doi: 10.1016/0198-0149(81)90091-1

Demol, M. (2024, December). *margot-demol/historical_analysis: Codes for the related publication : " Diagnosis of the Ocean Near-surface Horizontal Momentum Balance from pre-SWOT altimetric data, drifter trajectories and wind reanalysis".* Zenodo. Retrieved 2024-12-18, from https://zenodo.org/records/14513262 doi: 10.5281/zenodo.14513262

Dufau, C., Orsztynowicz, M., Dibarboure, G., Morrow, R., & Le Traon, P.-Y. (2016). Mesoscale resolution capability of altimetry: Present and future. *Journal of Geophysical Research: Oceans*, *121*(7), 4910–4927. (Publisher: Wiley Online Library)

Efron, B., & Tibshirani, R. J. (1994). *An Introduction to the Bootstrap.* New York: Chapman and Hall/CRC. doi: 10.1201/9780429246593

Ekman, & Vagn Walfrid. (1905). On the influence of the earth's rotation on ocean-currents.

Elipot, & Wenegrat. (2021). Vertical structure of near-surface currents – Importance, state of knowledge, and measurement challenges. *CLIVAR Variations*, *19*(1), 1–9.

Elipot, S., Lumpkin, R., Perez, R. C., Lilly, J. M., Early, J. J., & Sykulski, A. M. (2016). A global surface drifter data set at hourly resolution. *Journal of Geophysical Research: Oceans*, *121*(5), 2937–2966. (LU)

European Union-Copernicus Marine Service. (2021a). *GLOBAL OCEAN ALONG-TRACK L3 SEA SURFACE HEIGHTS REPROCESSED (1993-ONGOING) TAILORED FOR DATA ASSIMILATION.* Mercator Ocean International. Retrieved 2024-07-16, from https://resources.marine.copernicus.eu/product-detail/SEALEVEL_GLO_PHY_L3_MY_008_062/INFORMATION doi: 10.48670/MOI-00146

European Union-Copernicus Marine Service. (2021b). *GLOBAL OCEAN GRIDDED L4 SEA SURFACE HEIGHTS AND DERIVED VARIABLES REPROCESSED (1993-ONGOING).* Mercator Ocean International. Retrieved 2024-07-16, from https://resources.marine.copernicus.eu/product-detail/SEALEVEL_GLO_PHY_L4_MY_008_047/INFORMATION doi: 10.48670/MOI-00148

Ferrari, R. (2011). A frontal challenge for climate models. *Science*, *332*(6027), 316–317. (Publisher: American Association for the Advancement of Science)

Flexas, M. M., Thompson, A. F., Torres, H. S., Klein, P., Farrar, J. T., Zhang, H., & Menemenlis, D. (2019). Global Estimates of the Energy Transfer From the Wind to the Ocean, With Emphasis on Near-Inertial Oscillations. *Journal of Geophysical Research: Oceans*, *124*(8), 5723–5746. Retrieved 2024-04-26, from https://onlinelibrary.wiley.com/doi/abs/10.1029/2018JC014453 (_eprint: https://onlinelibrary.wiley.com/doi/pdf/10.1029/2018JC014453) doi: 10.1029/2018JC014453

Fox-Kemper, B., Danabasoglu, G., Ferrari, R., Griffies, S. M., Hallberg, R. W., Holland, M. M., ... Samuels, B. L. (2011, January). Parameterization of mixed layer eddies. III: Implementation and impact in global ocean climate simulations. *Ocean Modelling*, *39*(1), 61–78. Retrieved 2024-07-11, from https://www.sciencedirect.com/science/article/pii/S1463500310001290 doi: 10.1016/j.ocemod.2010.09.002

Fu, L.-L., Pavelsky, T., Cretaux, J.-F., Morrow, R., Farrar, J. T., Vaze, P., ... Dibarboure, G. (2024). The Surface Water and Ocean Topography Mission: A Breakthrough in Radar Remote Sensing of the Ocean and Land Surface Water. *Geophysical Research Letters*, *51*(4), e2023GL107652. Retrieved 2024-06-14, from https://onlinelibrary.wiley.com/doi/abs/10.1029/2023GL107652 (_eprint: https://onlinelibrary.wiley.com/doi/pdf/10.1029/2023GL107652) doi: 10.1029/2023GL107652

Johnson, E. S., & Luther, D. S. (1994). Mean zonal momentum balance in the upper and central equatorial Pacific Ocean. *Journal of Geophysical Research: Oceans*, *99*(C4), 7689–7705. Retrieved 2024-05-02, from https://onlinelibrary.wiley.com/doi/abs/10.1029/94JC00033 (_eprint: https://onlinelibrary.wiley.com/doi/pdf/10.1029/94JC00033) doi: 10.1029/94JC00033

Lilly, J. M., & Elipot, S. (2021). A Unifying Perspective on Transfer Function Solutions to the Unsteady Ekman Problem. *Fluids*, *6*(2), 85. (Publisher: Multidisciplinary Digital Publishing Institute)

Liu, Y., Jing, Z., & Wu, L. (2019). Wind Power on Oceanic Near-Inertial Oscillations in the Global Ocean Estimated From Surface Drifters. *Geophysical Research Letters*, *46*(5), 2647–2653. Retrieved 2023-07-10, from https://onlinelibrary.wiley.com/doi/abs/10.1029/2018GL081712 (_eprint: https://onlinelibrary.wiley.com/doi/pdf/10.1029/2018GL081712) doi: 10.1029/2018GL081712

Lévy, M., Franks, P. J., & Smith, K. S. (2018). The role of submesoscale currents in structuring marine ecosystems. *Nature communications*, *9*(1), 1–16. (Publisher: Nature Publishing Group)

Maximenko, N., Niiler, P., Centurioni, L., Rio, M.-H., Melnichenko, O., Chambers, D., ... Galperin, B. (2009, September). Mean Dynamic Topography of the Ocean Derived from Satellite and Drifting Buoy Data Using Three Different Techniques. *Journal of Atmospheric and Oceanic Technology*, *26*(9), 1910–1919. Retrieved 2023-12-22, from https://journals.ametsoc.org/view/journals/atot/26/9/2009jtecho672_1.xml (Publisher: American Meteorological Society Section: Journal of Atmospheric and Oceanic Technology) doi: 10.1175/2009JTECHO672.1

Mulet, S., Rio, M.-H., Etienne, H., Artana, C., Cancet, M., Dibarboure, G., ... Strub, P. T. (2021, June). The new CNES-CLS18 global mean dynamic topography. *Ocean Science*, *17*(3), 789–808. Retrieved 2023-12-20, from https://os.copernicus.org/articles/17/789/2021/ (Publisher: Copernicus GmbH) doi: 10.5194/os-17-789-2021

Nadarajah, S., & Pogány, T. K. (2016, February). On the distribution of the product of correlated normal random variables. *Comptes Rendus Mathematique*, *354*(2), 201–204. Retrieved 2024-05-14, from https://www.sciencedirect.com/science/article/pii/S1631073X15002873 doi: 10.1016/j.crma.2015.10.019

Niiler, P. P., Maximenko, N. A., & McWilliams, J. C. (2003, November). Dynamically balanced absolute sea level of the global ocean derived from near-surface velocity observations: ABSOLUTE SEA LEVEL OF THE GLOBAL OCEAN. *Geophysical Research Letters*, *30*(22). Retrieved 2022-12-22, from http://doi.wiley.com/10.1029/2003GL018628 doi: 10.1029/2003GL018628

Portabella, M., Trindade, A., Grieco, G., & Makarova, E. (2021). World Ocean Circulation Product User Manual for ERAstar v1. 0. (Publisher: European Space Agency)

Poulain, P.-M., Gerin, R., Mauri, E., & Pennel, R. (2009). Wind effects on drogued and undrogued drifters in the eastern Mediterranean. *Journal of Atmospheric and Oceanic Technology*, *26*(6), 1144–1156. (Publisher: American Meteorological Society)

Quilfen, Y., Piolle, J.-F., & Chapron, B. (2022). Towards improved analysis of short mesoscale sea level signals from satellite altimetry. *Earth System Science Data*, *14*(4), 1493–1512. (Publisher: Copernicus GmbH)

Rio, M. H., Guinehut, S., & Larnicol, G. (2011, July). New CNES-CLS09 global mean dynamic topography computed from the combination of GRACE data, altimetry, and in situ measurements. *Journal of Geophysical Research: Oceans*, *116*(C7), 2010JC006505. Retrieved 2022-12-22, from https://onlinelibrary.wiley.com/doi/10.1029/2010JC006505 doi: 10.1029/2010JC006505

Rio, M.-H., & Hernandez, F. (2004). A mean dynamic topography computed over the world ocean from altimetry, in situ measurements, and a geoid model. *Journal of Geophysical Research: Oceans*, *109*(C12). (Publisher: Wiley Online Library)

Rio, M.-H., Mulet, S., & Picot, N. (2014, December). Beyond GOCE for the ocean circulation estimate: Synergetic use of altimetry, gravimetry, and in situ data provides new insight into geostrophic and Ekman currents: Ocean circulation beyond GOCE. *Geophysical Research Letters*, *41*(24), 8918–8925. Retrieved 2022-12-22, from http://doi.wiley.com/10.1002/2014GL061773 doi: 10.1002/2014GL061773

Röhrs, J., Sutherland, G., Jeans, G., Bedington, M., Sperrevik, A. K., Dagestad, K.-F., … LaCasce, J. H. (2023, January). Surface currents in operational oceanography: Key applications, mechanisms, and methods. *Journal of Operational Oceanography*, *16*(1), 60–88. Retrieved 2023-12-15, from https://doi.org/10.1080/1755876X.2021.1903221 (Publisher: Taylor & Francis _eprint: https://doi.org/10.1080/1755876X.2021.1903221) doi: 10.1080/1755876X.2021.1903221

Spydell, M. S., Feddersen, F., & Macmahan, J. (2019, November). The Effect of Drifter GPS Errors on Estimates of Submesoscale Vorticity. *Journal of Atmospheric and Oceanic Technology*, *36*(11), 2101–2119. Retrieved 2023-02-09, from https://journals.ametsoc.org/view/journals/atot/36/11/jtech-d-19-0108.1.xml (Publisher: American Meteorological Society Section: Journal of Atmospheric and Oceanic Technology) doi: 10.1175/JTECH-D-19-0108.1

Stammer, D., & Cazenave, A. (2017). *Satellite altimetry over oceans and land surfaces.* CRC press.

Taylor, J. R., & Ferrari, R. (2011). Ocean fronts trigger high latitude phytoplankton blooms. *Geophysical Research Letters*, *38*(23). Retrieved 2024-03-04, from https://onlinelibrary.wiley.com/doi/abs/10.1029/2011GL049312 (_eprint: https://onlinelibrary.wiley.com/doi/pdf/10.1029/2011GL049312) doi: 10.1029/2011GL049312

Trindade, A., Grieco, G., Makarova, E., & Portabella, M. (2022, April). *WOC ERA* Hourly Global Stress Equivalent Wind and Wind Stress (V.2.0) [Dataset].* CSIC - Instituto de Ciencias del Mar (ICM). Retrieved 2024-07-16, from https://digital.csic.es/handle/10261/330890 doi: 10.20350/DIGITALCSIC/15436

Trindade, A., Portabella, M., Stoffelen, A., Lin, W., & Verhoef, A. (2020, February). ERAstar: A High-Resolution Ocean Forcing Product. *IEEE Transactions on Geoscience and Remote Sensing*, *58*(2), 1337–1347. Retrieved 2022-12-22, from https://ieeexplore.ieee.org/document/8879669/ doi: 10.1109/TGRS.2019.2946019

Yu, X., Garabato, A. C. N., Martin, A. P., Buckingham, C. E., Brannigan, L., & Su, Z. (2019, June). An Annual Cycle of Submesoscale Vertical Flow and Restratification in the Upper Ocean. *Journal of Physical Oceanography*, *49*(6), 1439–1461. Retrieved 2024-04-26, from https://journals.ametsoc.org/view/journals/phoc/49/6/jpo-d-18-0253.1.xml (Publisher: American Meteorological Society Section: Journal of Physical Oceanography) doi: 10.1175/JPO-D-18-0253.1

Yu, X., Ponte, A. L., Elipot, S., Menemenlis, D., Zaron, E. D., & Abernathey, R. (2019). Surface kinetic energy distributions in the global oceans from a high-resolution numerical model and surface drifter observations. *Geophysical Research Letters*, *46*(16), 9757–9766. (Publisher: Wiley Online Library)

Yu, X., Ponte, A. L., Lahaye, N., Caspar-Cohen, Z., & Menemenlis, D. (2021, October). Geostrophy Assessment and Momentum Balance of the Global Oceans in a Tide- and Eddy-Resolving Model. *Journal of Geophysical Research: Oceans*, *126*(10). Retrieved 2022-12-22, from https://onlinelibrary.wiley.com/doi/10.1029/2021JC017422 doi: 10.1029/2021JC017422